Supplementary Information: IF2 aptamers allosterically impair bacterial translation initiation

Lesia Tello[1], Katherin Peñaranda[1,2,†,*], Ana Sanchez-Castro[1,†], Joaquin Rodriguez Trelles[1,3], Victor Barrenechea[1], Daria S. Vinogradova[4,5], Pablo D. Dans[6,7], Alena Paleskava[8,9], Andrey L. Konevega[4,8,9], Roberto Spurio[2], and Pohl Milon[1,*]

[1]Laboratory of Biomolecules, Faculty of Health Sciences, Universidad Peruana de Ciencias Aplicadas (UPC), Lima 15023, Peru

[2]School of Biosciences and Veterinary Medicine, University of Camerino, Camerino 62032, Italy.

[3]School of Biology, Faculty of Health Sciences, Universidad Peruana de Ciencias Aplicadas (UPC), Lima 15023, Peru

[4]Petersburg Nuclear Physics Institute named by B.P. Konstantinov of National Research Centre “Kurchatov Institute”, Gatchina 188300, Russia

[5]Nanotemper Technologies Rus, Saint Petersburg 191167, Russia

[6]Department of Biological Sciences, CENUR Litoral Norte, Universidad de la República, Salto 50000, Uruguay.

[7]Bioinformatics Unit, Institut Pasteur de Montevideo, Montevideo 11400, Uruguay

[8]Peter the Great St. Petersburg Polytechnic University, Saint Petersburg 195251, Russia

[9]National Research Centre “Kurchatov Institute”, Moscow 123182, Russia

*Correspondence to: katherin.penaranda@upc.pe and pmilon@upc.edu.pe

[†]These authors contributed equally to this work.

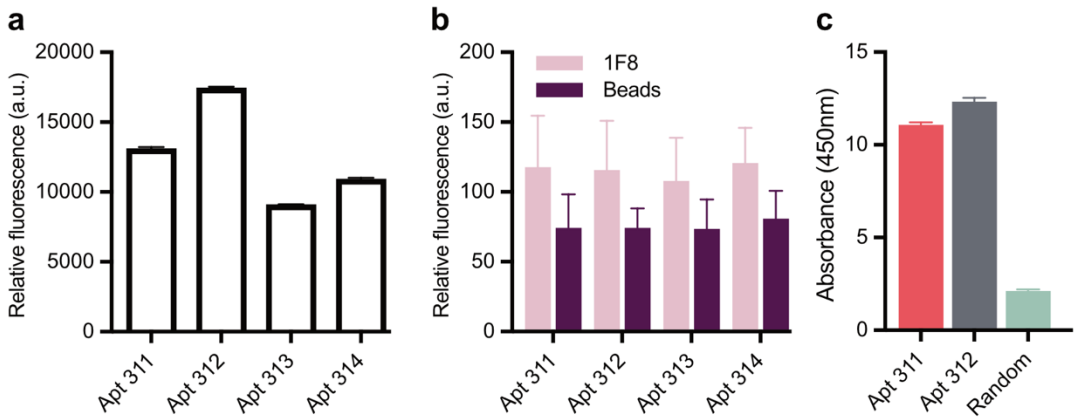

Supplementary Figure S1. Screening assays of four candidate aptamers. Pull-down assays evaluating aptamer recovery after binding to His-tagged IF2, 1F8, and Ni-NTA magnetic beads. Fluorescent aptamers (1 µM) were incubated with proteins (1 µM) and recovered using Ni-NTA beads. Fluorescence in the eluate was quantified as relative fluorescence units using a microplate reader. (**a**) IF2-dependent pull-down assays. (**b**) Control protein assays. Because the fluorescence scale differed between (**a**) and (**b**), the data are shown separately albeit the experiments were performed together. (**c**) Aptamer binding to IF2 comparison with a random oligonucleotide. Binding to IF2γ was tested with the specific aptamers (Apt 311 and Apt 312) and, in parallel, with a random DNA oligonucleotide of equivalent length used as a nonspecific control. IF2γ (1 µM) was immobilized on a solid surface and incubated with each DNA. Bound DNA was detected through a streptavidin–HRP enzymatic reaction using TMB (3,3′,5,5′-tetramethylbenzidine) as substrate. Absorbance was measured at 450 nm after 30 min. Data represent mean ± s.d. from triplicate experiments.

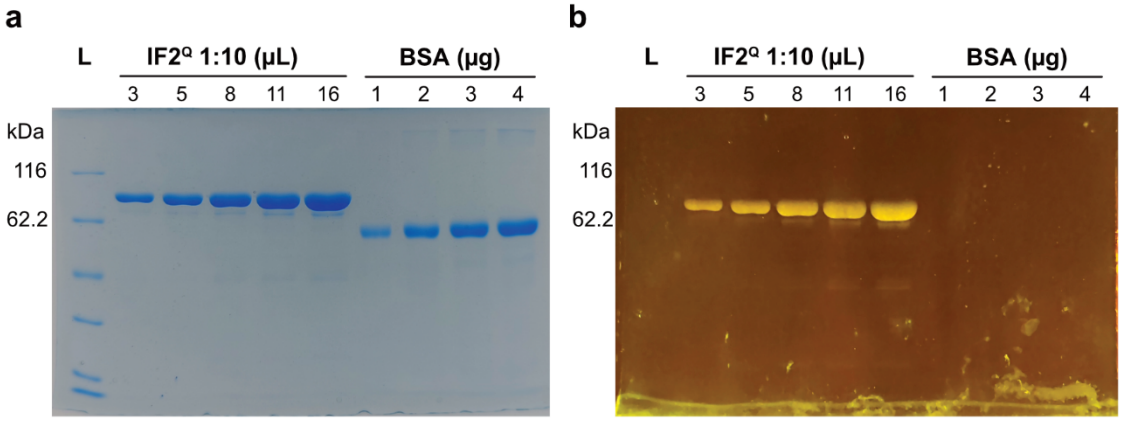

Supplementary Figure S2. Purification and fluorescent labelling of IF2γ G810C. (**a**) Coomassie stained 10% SDS–PAGE of labelled IF2γ G810C with quencher fluorophore Atto 540Q ($IF2^{Q}$). A 1:10 dilution of a 45 µM $IF2^{Q}$ was prepared and increasing volumes were loaded to assess protein detection and labelling efficiency. BSA was included as a standard for band intensity comparison. (**b**) The same gel shown in (**a**) but observed under UV light before staining.

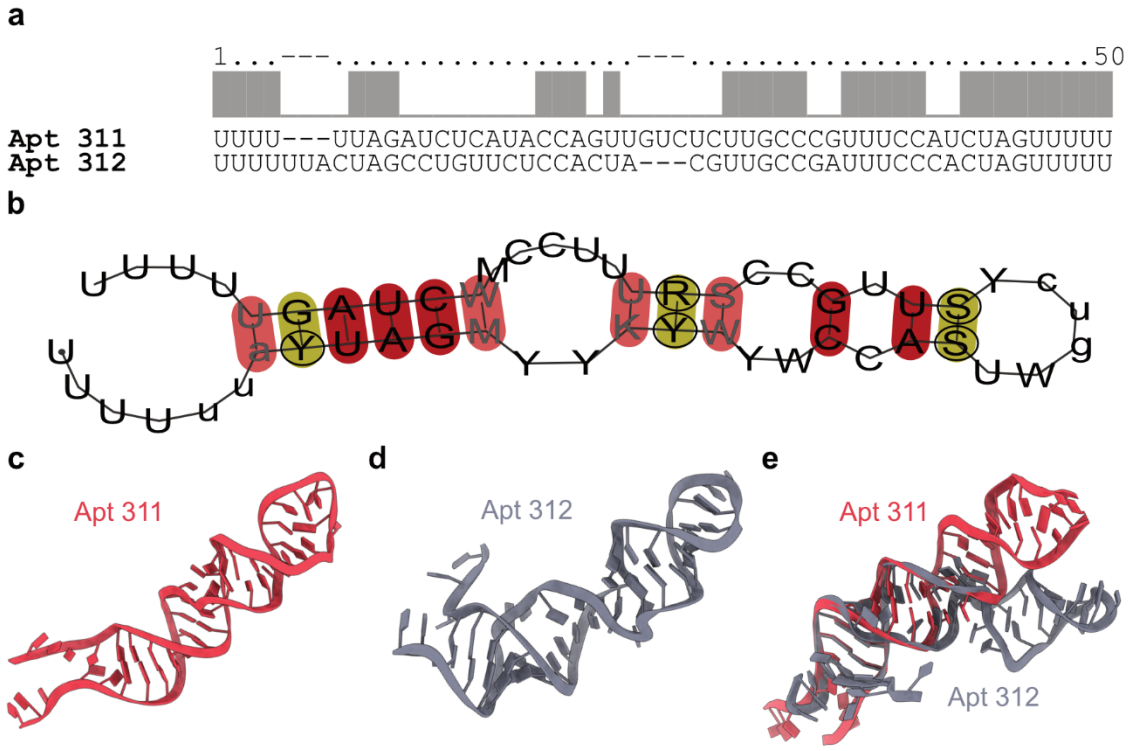

Supplementary Figure S3. Sequence alignment and structural models of Apt 311 and Apt 312. (**a**) Sequence alignment performed using Clustal Omega (version 1.2.4; http://www.clustal.org/omega/)[1]. Grey bars indicate conserved regions (29 out of 50 nucleotides) shared between the two aptamers. (**b**) Consensus secondary structure alignment predicted using LocARNA (Freiburg RNA Tools; http://rna.informatik.uni-freiburg.de/LocARNA, accessed 28 January 2026)[2–4]. The colour scheme follows the LocARNA/RNAalifold convention and shows two aspects of conservation. Hue indicates sequence conservation (red = a single base-pair type; warmer hues such as yellow = variation among compatible base-pair types), whereas colour saturation indicates structural conservation (paler shades reflect more incompatible base pairs). Nucleotides are represented using the IUPAC ambiguity code. (**c–e**) Structural modelling and comparative alignment of Apt 311 and Apt 312. Individual 3D representations of (**c**) Apt 311 (red), and (**d**) Apt 312 (grey) visualized in UCSF ChimeraX (version 1.10.1, build 2025-07-24; https://www.rbvi.ucsf.edu/chimerax)[5]. (**e**) **Structural superposition** via the Needleman–Wunsch algorithm[6] highlights a highly conserved scaffold. While distal flexibility resulted in a global RMSD of 20.318 Å, the optimized alignment of the structural core (pruned atom pairs) yielded an RMSD of 0.802 Å, confirming a shared 3D motif between both variants.

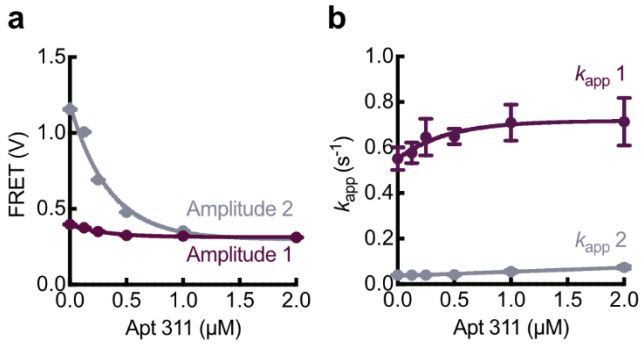

Supplementary Figure S4. Two-step reaction analysis of fMet-tRNA^{Flu} binding. (**a**) Dependence of amplitude 1 (purple) and amplitude 2 (grey) on Apt 311 concentration. (**b**) Apparent constants (k_{app}) of Apt 311-mediated fMet-tRNA^{Flu} binding. Dependence of k_{app} 1 (purple) and k_{app} 2 (grey) on Apt 311 concentration obtained from the analysis of Apt 311 titration (**Fig. 3c**).

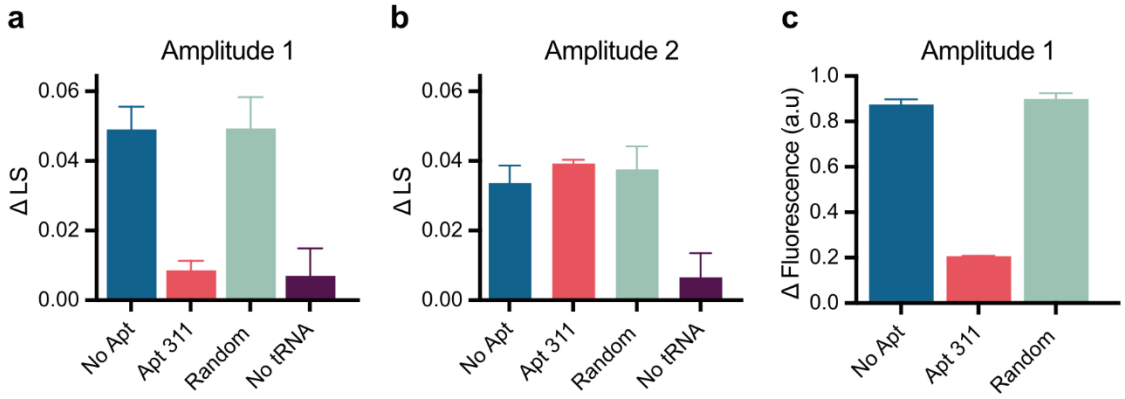

Supplementary Figure S5. Amplitudes of time traces from the concomitant binding of fMet-tRNA^{fMet} and the 50S subunit to the 30S PIC (**Fig. 4c–d**). (**a–b**) are monitored by light scattering and (**c**) by fluorescence using Bpy-Met-tRNA^{fMet}. The effect of Apt 311 (red) was compared to controls without aptamer (blue), with random DNA (green), and without fMet-tRNA^{fMet} (purple). Amplitude 1 from both assays is drastically reduced by the presence of Apt 311, while amplitude 2 was not affected. Amplitudes are the average of 5–7 replicates; two-phase non-linear fitting was applied for all conditions, except (**c**) in the presence of Apt 311 (red) where a one-phase non-linear fitting was applied.

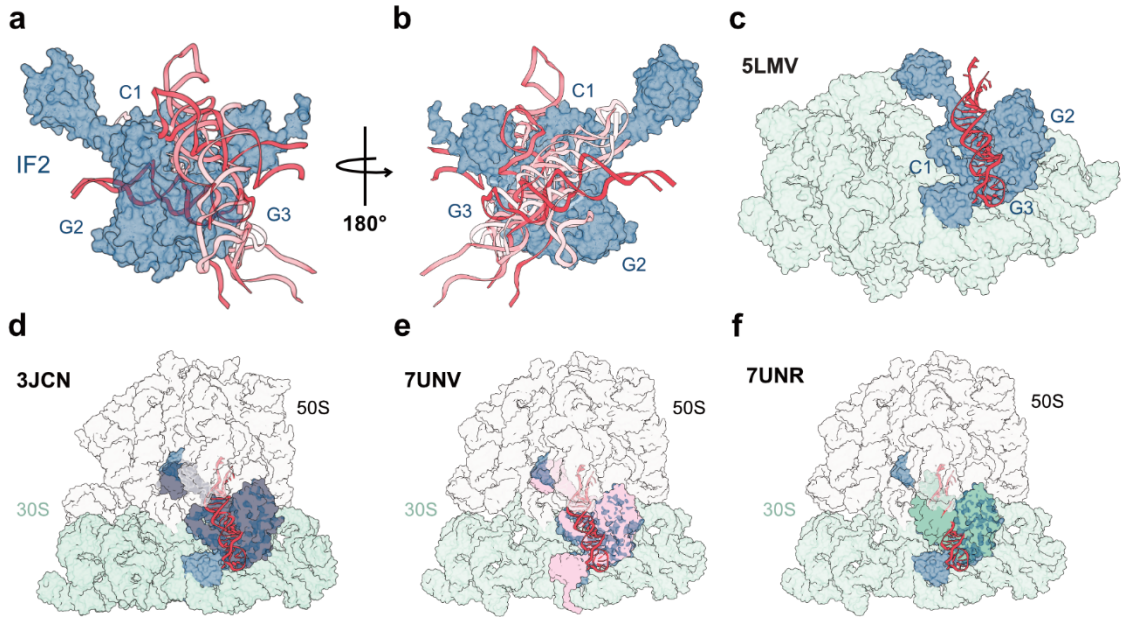

Supplementary Figure S6. Structural basis of Apt 311 binding and potential steric inhibition inferred from ribosomal superposition. (**a, b**) Orthogonal views of the top-ranked docking models (Top 10) generated with the HDOCK server (http://hdock.phys.hust.edu.cn, accessed 17 October 2025)[7,8], showing Apt 311 (red) bound to IF2 (blue) at the G2, G3, and C1 domains. (**c**) Superposition in UCSF ChimeraX version 1.10.1 (https://www.rbvi.ucsf.edu/chimerax/)[5] of the IF2–aptamer complex onto the native 30S ribosomal subunit (PDB 5LMV) shows that aptamer binding is compatible with 30S association, with no detectable steric clashes. (**d–f**) Structural alignments of the docking model with full 70S ribosome structures reveal clashes with the 50S subunit: (**d**) *E. coli* 70S (PDB: 3JCN; pruned RMSD = 0.982 Å), where the IF2 of the model is shown in grey; (**e**) *Pseudomonas aeruginosa* 70S containing inactive, GDP-bound IF2 (PDB 7UNR; global RMSD = 21.914 Å), where the IF2 of the model is shown in pink; and (**f**) *P. aeruginosa* 70S containing active, GTP-bound IF2 (PDB 7UNV; pruned RMSD = 0.887 Å), where the IF2 of the model is shown in green.

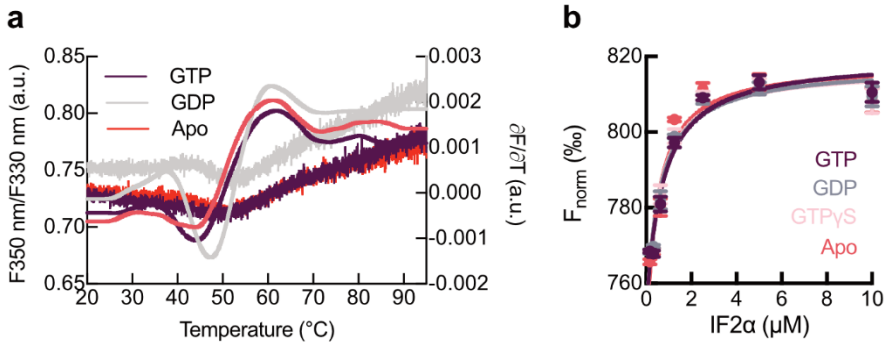

Supplementary Figure S7. Impact of guanosine nucleotides on IF2 and on Apt 311-Cy5 binding. (**a**) Nucleotide-dependent thermal stability of IF2 measured by nano differential scanning fluorimetry (nanoDSF). Thermal unfolding of IF2 was followed in the apo state (red), bound to GTP (purple) and bound to GDP (grey). For each condition the ratio of intrinsic fluorescence at 350 and 330 nm (F350/F330, left axis) and its first derivative ($\partial F/\partial T$, right axis) are plotted against temperature. The maximum of $\partial F/\partial T$ marks the melting temperature (Tm) of the unfolding transition. (**b**) Binding curve of Apt 311-Cy5 to IF2 in the presence of 100 µM nucleotides (GTP, GDP and GTPγS) and in the apo state. Normalized fluorescence (Fnorm ‰) was used for K_d determination by non-linear hyperbolic fitting. K_d values in µM were determined as follows: GTP (0.71 ± 0.16), GDP (0.60 ± 0.14), GTPγS (0.54 ± 0.15), and apo (0.48 ± 0.14). Error bars represent s.d. from 2 replicates and 3 intra-assay repetitions.

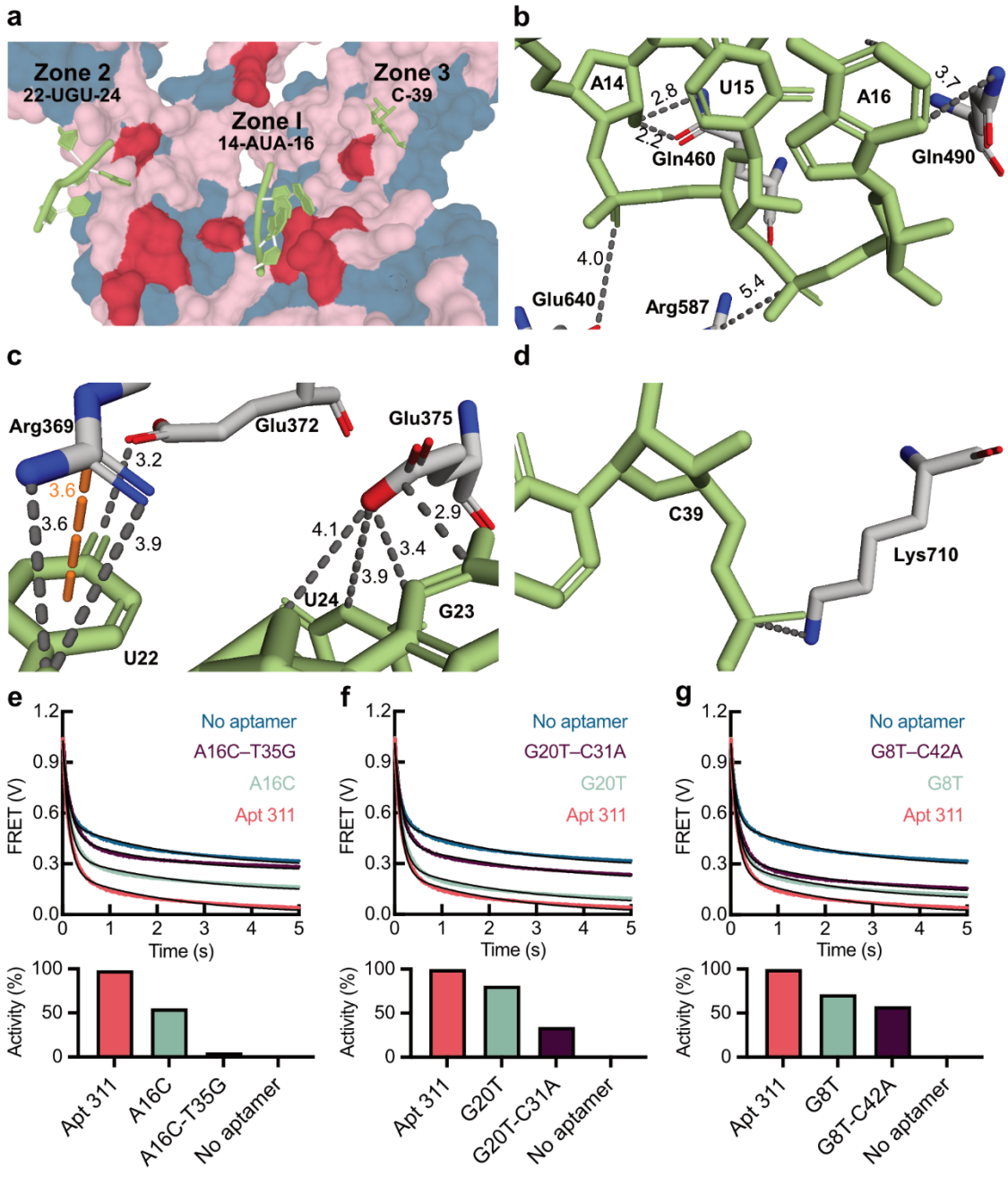

Supplementary Figure S8. Functional and structural stability analysis of Apt 311 mutants. (**a**) Protein–nucleic acid interactions were analysed with PLIP (2025 release; https://plip-tool.biotec.tu-dresden.de, accessed 7 April 2026)[9]; the resulting interaction model was derived from the top-ranked Apt 311 docking model and rendered in PyMOL (version 3.1.7.2; Schrödinger, LLC)[10]. Different interaction types between the aptamer and IF2 were identified, defining three major binding interfaces: Zone I (AUA Anchor), the AUA motif spanning nucleotides A14–A16; Zone II (UGU Patch), the UGU motif at positions U22–U24; and Zone III (Distal Clamp), centred on C39. Motif names and residue identities follow the RNA-based model used for the structural prediction and the PLIP analysis; because the aptamers are DNA, each uridine corresponds to the equivalent thymidine (AUA = ATA, A14–T15–A16; UGU = TGT, T22–T24). In the figure, nucleotides belonging to these three zones are shown in green together with the

predicted hotspots (red) and interaction regions (pink) derived from the ten docking models. Zone I directly overlaps with a hotspot, whereas Zones II and III are located adjacent to frequent interaction regions**.** (**b**) Detailed view of Zone I. In this model A14 acts as the primary anchoring residue, establishing a 2.25 Å hydrogen bond with Gln460. U15 and A16 further contribute to a stable interaction network through hydrogen bonds with Glu640 and Gln490, respectively. (**c**) Detailed view of Zone II. Binding in this region is stabilized by a hydrogen-bond and π-cation network, primarily driven by contacts between Arg369 and U22, together with interactions involving Glu372 and Glu375. (**d**) Close-up view of Zone III. The distal interface is stabilized by a specific contact between aptamer residue C39 and Lys710 of IF2. (**e–g**) Binding of $IF2^{Q}$ to a 30S–$IF1^{flu}$–IF3 complex was measured by FRET in a stopped-flow system. The single- and double-mutant aptamers were pre-bound to $IF2^{Q}$. Aptamer activity inhibition (%) was calculated considering the Apt 311 as 100% while the No aptamer amplitude as 0% inhibition.

References

1. Sievers, F. et al. Fast, scalable generation of high-quality protein multiple sequence alignments using Clustal Omega. Mol. Syst. Biol. **7**, 539 (2011).

2. Will, S., Joshi, T., Hofacker, I. L., Stadler, P. F. & Backofen, R. LocARNA-P: accurate boundary prediction and improved detection of structural RNAs. RNA **18**, 900–914 (2012).

3. Will, S., Reiche, K., Hofacker, I. L., Stadler, P. F. & Backofen, R. Inferring non-coding RNA families and classes by means of genome-scale structure-based clustering. PLoS Comput. Biol. **3**, e65 (2007).

4. Raden, M. et al. Freiburg RNA tools: a central online resource for RNA-focused research and teaching. Nucleic Acids Res. **46**, W25–W29 (2018).

5. Meng, E. C. et al. UCSF ChimeraX: tools for structure building and analysis. Protein Sci. **32**, e4792 (2023).

6. Needleman, S. B. & Wunsch, C. D. A general method applicable to the search for similarities in the amino acid sequence of two proteins. J. Mol. Biol. **48**, 443–453 (1970).

7. Yan, Y., Zhang, D., Zhou, P., Li, B. & Huang, S.-Y. HDOCK: a web server for protein–protein and protein–DNA/RNA docking based on a hybrid strategy. Nucleic Acids Res. **45**, W365–W373 (2017).

8. Yan, Y., Tao, H., He, J. & Huang, S.-Y. The HDOCK server for integrated protein–protein docking. Nat. Protoc. **15**, 1829–1852 (2020).

9. Schake, P., Bolz, S. N., Linnemann, K. & Schroeder, M. PLIP 2025: introducing protein–protein interactions to the protein–ligand interaction profiler. Nucleic Acids Res. **53**, W463–W465 (2025).

10. The PyMOL Molecular Graphics System, Version 3.1.7.2, Schrödinger, LLC.